Ion intercalation engineering of electronic properties of two-dimensional crystals of 2H-$TaSe_2$

Yueshen Wu,[1] Hui Xing,[1,*] Chao-Sheng Lian,[2] Hailong Lian,[1] Jiaming He,[1]
Wenhui Duan,[3] Jinyu Liu,[4] Zhiqiang Mao,[5] and Ying Liu[1,5,6,†]

[1]*Key Laboratory of Artificial Structures and Quantum Control and Shanghai Center for Complex Physics, School of Physics and Astronomy, Shanghai Jiao Tong University, Shanghai 200240, China*

[2]*International Laboratory for Quantum Functional Materials of Henan and School of Physics and Engineering, Zhengzhou University, Zhengzhou 450001, China*

[3]*Department of Physics and State Key Laboratory of Low-Dimensional Quantum Physics, Tsinghua University, Beijing 100084, China*

[4]*Department of Physics and Engineering Physics, Tulane University, New Orleans, Louisiana 70118, USA*

[5]*Department of Physics and Materials Research Institute, Pennsylvania State University, University Park, Pennsylvania 16802, USA*

[6]*Collaborative Innovation Center of Advanced Microstructures, Nanjing 210093, China*

(Received 6 August 2019; published 28 October 2019)

Ion intercalation was recently used to explore two-dimensional (2D) transition metal dichalcogenides (TMDs) with precise tuning of ion concentration in a field-effect-transistor configuration. However, how to systematically change the properties of 2D TMDs, e.g., superconductivity and charge density waves, by ion intercalation has not been explored. We report in this paper results of electrical transport measurements on 2D crystals of 2H-$TaSe_2$ intercalated with Li ions that is tuned continuously by ionic gating. Shubnikov–de Haas magnetoconductance oscillation and Hall coefficient measurements on crystals of 2H-$TaSe_2$ revealed an ion intercalation induced multi- to single-band change in the Fermi surface (FS) topology, deep in the charge density wave phase, resulting in a reduction of the number of independent channels for electronic conduction. A remarkable crossover from weak antilocalization to weak localization tuned by gate voltage or temperature was found and attributed to the ion intercalation induced variations in the spin-orbital coupling and electron-phonon interaction. These observations provide new insight into the enhancement of superconductivity and the suppression of charge density waves in 2D 2H-$TaSe_2$ induced by ion intercalation and demonstrate furthermore the great potential of ion intercalation for engineering electronic properties of 2D TMDs.

DOI: 10.1103/PhysRevMaterials.3.104003

I. INTRODUCTION

Motivated by the broad need to develop battery-based energy storage technologies, ion intercalation into materials suitable for these applications has been pursued intensively in recent years. Layered transition metal dichalcogenides (TMD) featuring a van der Waals interlayer coupling are capable of hosting ions in its various interstitial sites, making TMDs an important class of electronic materials for ion intercalation studies. In this regard, intercalation of organic molecular ions in layered TMDs was used to systematically increase the spacing between the layered unit cells to infer the intrinsic properties of the monolayer TMD [1]. The discovery of mechanical exfoliation preparation of single-unit-cell crystals of TMD have not only made true monolayer materials widely available, but also opened new directions of research ranging from the valley Hall effect [2], to Ising superconductivity [3,4], to topological quantum spin Hall effect [5–8].

Intercalating ions of a metal into an electronic material, on the other hand, renders material engineering of different aspects, including the electron/ion conduction [9], optical [10], and electrochemical [11,12] properties. For example, it was found that intercalating Li ions into $SmNiO_3$ suppresses the electronic conduction and enhances the ionic conduction simultaneously through the formation of a nonconducting phase of a Mott insulator [13–15], demonstrating an approach to an enhanced ionic conduction. Intercalating Cu ions into $TiSe_2$ was found to suppress the critical temperature of charge density wave (CDW) and induce superconductivity (SC), most likely by enhancing the effect of electronic correlations [16], adding a fundamental science aspect to the ion intercalation studies of TMDs.

Hexagonal $TaSe_2$, referred to as 2H-$TaSe_2$, featuring an ABAB stacking, where A and B each represents a Se-Ta-Se trilayer stack, is a metallic TMD possessing both CDW and SC orders. While the SC order in the bulk was found only at very low temperatures, $T_c^{SC} = 0.15$ K [17], a CDW order occurs below $T_c^{CDW} = 122$ K (with an additional lock-in transition at 90 K) [18,19], the highest among metallic 2H-TMDs [20]. Because of the very high T_c^{CDW}, this material has been an important CDW material for addressing the outstanding issues concerning the formation of CDW, as well as the interplay between CDW and SC.

The effect of ion intercalation on 2H-$TaSe_2$ properties has been studied previously. Intercalation of Na or Cs [21] and K ions [22] into 2H-$TaSe_2$ were found to change the

*huixing@sjtu.edu.cn
†yxl15@psu.edu

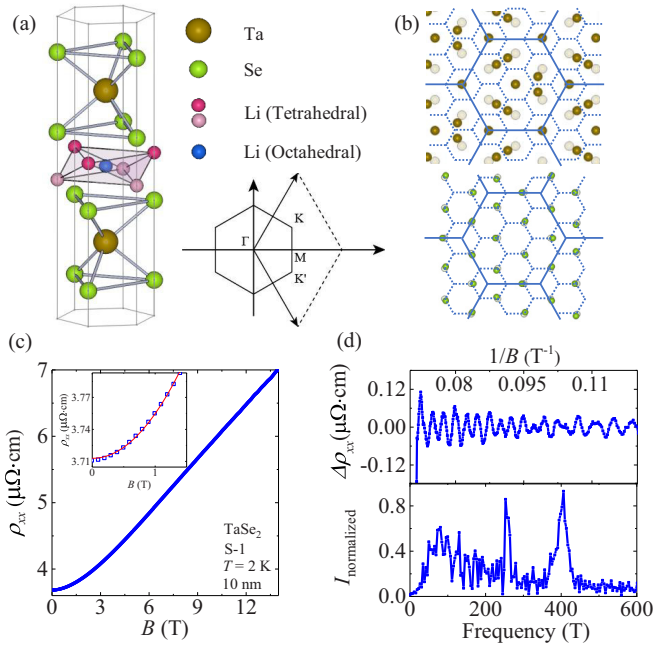

FIG. 1. Sample characterization. (a) Illustration of Li intercalation into 2H-$TaSe_2$ and the first Brillouin zone. (b) Illustration of 3×3 CDW superlattice. (c) Longitudinal electrical resistivities of a 10-nm-thick crystal at 2 K with $B//c$. Inset: The low field dependent resistivity close to B^2 behavior. (d) Field dependent resistivity with a smooth background subtracted showing Shubnikov–de Haas oscillations (SdHO) and corresponding fast Fourier transform (FFT). Two frequencies of 253 and 407 T were obtained, corresponding to FS pockets centering the Γ and the K or K' points, respectively.

band structure and suppress CDW. For the Li intercalation of 2H-$TaSe_2$, Mössbauer spectroscopy [23] studies in the bulk also revealed a change in the valence of Ta, from Ta^{4+} to Ta^{3+}, suggesting bonding between Li and Se ions. Raman spectroscopy studies of 2H-$TaSe_2$ intercalated by organic molecules of $NH_2CH_2CH_2NH_2$ (EDA) revealed enhanced influence of the crystal lattice on CDW order [24]. Ionic conduction in a Li ion intercalated 2D crystal of 2H-$TaSe_2$ was measured in a partially covered ionic field effect transistor device, leading to the determination of the diffusion constant for the Li ions and insight into intercalation phases controlled reasonably reversibly by ionic gating [25]. However, no systematic studies of ion intercalation into 2H-$TaSe_2$ or any other TMDs aimed at manipulating their material properties including the interplay between CDW and SC in a device configuration, have been carried out.

II. RESULTS AND DISCUSSION

The normal-state crystal structure and the first Brillouin zone (BZ) of 2H-$TaSe_2$ are shown in Fig. 1(a). The formation of CDW is accompanied by a 3×3 reconstruction in the crystalline structure involving, interestingly, moving essentially only Ta ions, leaving the positions of Se ions largely unchanged [Fig. 1(b)]. This crystal reconstruction enlarges the size of the real-space unit cell but reduces that of the first Brillouin zone in the momentum space. Shubnikov–de Haas oscillation (SdHO) measurements showed that 2H-$TaSe_2$ features a FS of multiple energy bands [26]. While angle resolved photoemission spectroscopy (ARPES) studies of 2H-$TaSe_2$ also revealed a multiband FS in the CDW state [27,28], the two methods have failed to arrive at a self-consistent account of the FS topology, including the very basic question on the number of FS sheets. Basically, the crystal reconstruction and the associated bended bands as well as the lack of the first-principle calculation of the band structure, which is computationally unattainable, made the analysis of the SdHO and ARPES data very difficult [29].

We carried out electrical resistivity measurements on a 10-nm-thick, un-intercalated crystal of 2H-$TaSe_2$ as a function of the magnetic field at 2 K up to 14 T [Fig. 1(c)]. We observed the expected parabolic field dependence at low fields [inset of Fig. 1(c)] and Shubnikov–de Haas oscillations (SdHOs) high fields—these oscillations are evident only after a smooth background is subtracted [upper panel of Fig. 1(d)]. The SdHO frequencies determined by the peak position in our fast Fourier transformation (FFT) are 253 and 407 T [lower panel of Fig. 1(d)], close to the two of the many found previously, 258 and 396 T, respectively [26]. Our data suggest that the FS of this 10-nm-thick crystal is essentially the same as the bulk. Other frequencies seen in the bulk are missing in the 2D crystal data most likely due to its disorder stronger in 2D than in the bulk crystals.

Lithium ions were intercalated into a 10-nm-thick crystal of 2H-$TaSe_2$ in an ionic field effect transistor device [Fig. 2(a)]. It was shown previously that CDW was suppressed by the intercalation of Li ions as the gating voltage becomes sufficiently large. The Hall coefficient R_H, obtained from a 10-nm-thick crystal at 2 K, was found to be negative, depending on the field nonlinearly at low gate voltages V_G [Fig. 2(b)]. In addition to the CDW and impurities, the nonlinear dependence is most likely due to the multiband nature of the FS, with the electronlike bands dominating the Hall coefficient [30]. As the gate voltage increases, R_H was found to change its sign between $V_G = 0.8$ and 1.1 V. Furthermore, $R_H(H)$ curves obtained in gate voltages equal to or higher than 1.1 V show linear field dependence [Fig. 2(b)], suggesting that an ion intercalation induced change in the FS topology from multiple pockets to a single holelike one deep in the CDW phase [Fig. 2(c)]. It is interesting to note that the dramatic change in FS topology and the suppression of CDW do not occur at the same gate voltage, suggesting the occurrence of the CDW is most likely unrelated to FS nesting. We also carried out Raman spectroscopy measurements at room temperature on a 40-nm-thick crystal tuned by ionic gating induced ion intercalation (see the Supplemental Material (SM) [31]). We found that the Li ion intercalation leads to a dramatic change in the phonon spectrum featuring A_{1g} and E_{2g} modes [24] at the gate voltage closer to the change in FS topology but not the suppression of the CDW order.

Ion intercalation introduces disorder into the crystal, leading to quantum transport characterized by the effect of weak localization (WL) or weak antilocalization (WAL) depending on the strength of the spin-orbital coupling. For a 2D weakly disordered electronic system, Maekawa and Fukuyama (MF)

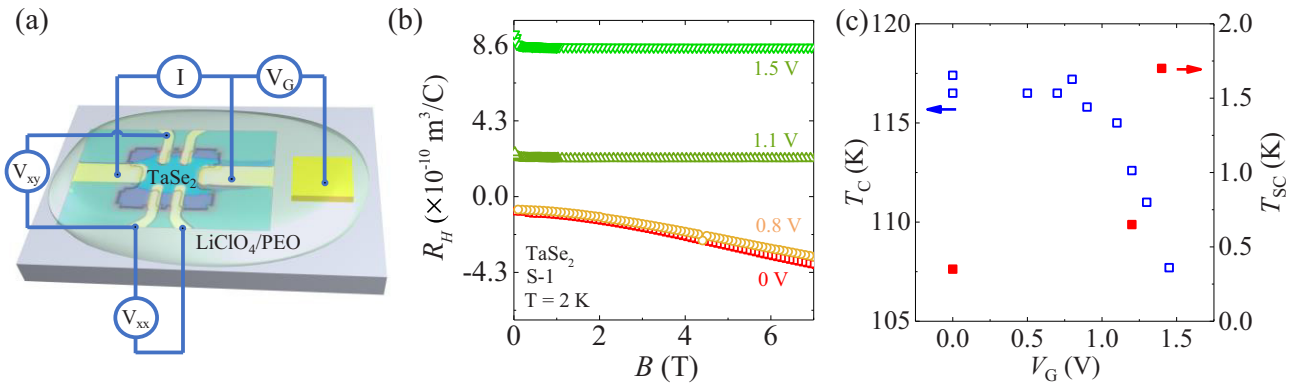

FIG. 2. Superconductivity and CDW. (a) Hybrid image of sample configuration and optical image of a real device. (b) Hall coefficient R_H as a function of magnetic field for the 10-nm-thick sample at various gate voltages for $V_G = 0$ and 0.8 V at 2 K showing that R_{xy} is negative and nonlinear and for $V_G = 1.1$ and 1.5 V showing that R_H is positive and magnetic field independent. (c) The gate voltage dependence of transition temperature of CDW and superconductivity [41].

calculated the field dependence of MC [32], yielding

$$\Delta\sigma(T,B) = \frac{Ne^2}{\pi h}\left\{F\left(\frac{B}{B_\phi + B_{so}}\right) - \frac{1}{2}\left[F\left(\frac{B}{B_\phi}\right) - F\left(\frac{B}{B_\phi + 2B_{so}}\right)\right]\right\} + aB^2, \quad (1)$$

where $F(z) = \psi(\frac{1}{2} + \frac{1}{z}) + \ln(z)$, B is the magnetic flux intensity, $\psi(z)$ is the digamma function, $B_\varphi = \hbar/4el_\varphi^2$ and $B_{so} = \hbar/4el_{so}^2$, with l_φ and l_{so} the inelastic scattering induced dephasing and spin-orbital scattering lengths $l_\varphi^2 = D\tau_\varphi$ and $l_{so}^2 = D\tau_{so}$, respectively, D is the diffusion constant, and N is the number of independent conduction channels [33]. The last term in Eq. (1) accounts for the background from the conventional MC, as found in the literature [34]. The N represents the multiband effects (see the SM [31]). In addition, the temperature dependence of σ_{WL} in zero field when only WL is present is given by [35]

$$\sigma_{WL} = \sigma(T) - \sigma_B = -C(e^2/\pi h)\ln(T/T_0), \quad (2)$$

where σ_B is the Boltzmann or classical conductance, C is a constant, e is the electron charge, and h is the Planck constant. Here $\sigma(T) - \sigma_B$ can be approximated by $\Delta R_s(T)/[R_s(T_0)]^2$, where $R_s(T)$ is the temperature dependent sheet resistance and T_0 is the temperature at which R_s reaches the minimum. In general, $C = Np + \gamma$, where N is the number of conduction channels following Ref. [18] (see below), the index p is related to the inelastic scattering induced dephasing time $\tau_\varphi(\tau_\varphi^{-1} \sim T^p)$ [36], and γ is a parameter characterizing the electron-electron scattering rate, with $t_{ee}^{-1} \sim T^\gamma$ [35,36]. These scattering times describe the properties of a metallic electronic material.

Experimentally, the MC of a 10-nm-thick crystal of 2H-$TaSe_2$ was found to be negative at low gate voltages, featuring distinctive $\sim B^2$ behavior at low fields [Fig. 3(a), upper panel] without WL or WAL. As V_G increased to 1.1 V, at which the Hall coefficient was found to change its sign [Fig. 2(b)]. Equation (1) was found to describe the MC data obtained at $V_G \geqslant 1.1$ V [Fig. 3(a), lower panel]. As the V_G increased, the WAL behavior in MC was found to be largely unchanged. However, at $V_G = 2.5$ V, MC is seen to first decrease and then increase again. At $V_G = 2.6$ V, fully positive MC was seen [Fig. 3(b)]. All this is consistent with the MF theory [32], with the change in the sign of MC an indication of a crossover from WAL to WL behavior. Fitting the MC data at each V_G to the MF theory led to gate voltage dependencies of l_φ and l_{so} [Fig. 3(c)]. When $l_\varphi > l_{so}$, the spin-orbit scattering dominates, leading to negative MC and WAL. However, when $l_\varphi < l_{so}$, the opposite is true. The WAL to WL crossover was also seen in the temperature dependence of the zero-field $\Delta\sigma$. As seen in Fig. 4(a), a crossover from metallic to weakly insulating behavior was observed as V_G was raised from 2.5 to 2.6 V, with the resistivity at $V_G = 2.6$ V depending on the temperature logarithmically as described in Eq. (2).

The best fit of the MF theory to our MC data for $V_G \geqslant 1.1$ V yielded a value of $N = 2$, including for those dominated by WL when $V_G = 2.6$ V. Interestingly, the temperature dependence of the sample conductivity at $V_G = 2.6$ V was found to be consistent with this result. Importantly, as inferred from the relative magnitudes of the corrections to the conductance and Hall coefficient, the electron-electron scattering contribution to the quantum correction of the sample conductance appears to be negligible (see the SM [31]). The coefficient in the logarithmic sample conductivity then becomes $C = Np$. The best fit to the data yielded a value of $C = 4.88 \pm 0.02$ at $V_G = 2.6$ V. The value $Np = 4.88$ obtained from fitting the $\sigma(T)$ at $V_G = 2.6$ V [Fig. 4(a)] will yield a value of $N = 2$ as an experimental value of $p \approx 2.5$ was found (see below). The same fitting to the MC data obtained on 3-nm-thick un-intercalated crystals yielded $N = 6$ [Fig. 4(b)]. Similarly, for the 10-nm-thick crystal, fitting the MC data obtained after V_G was swept back from 2.6 to 0 V [Fig. 4(c)], which was found to show WAL instead of $\sim B^2$ dominated behavior, presumably due to disorder caused by residual ions stuck in the crystal, also yielded $N = 6$. We note that a 12-nm-thick,

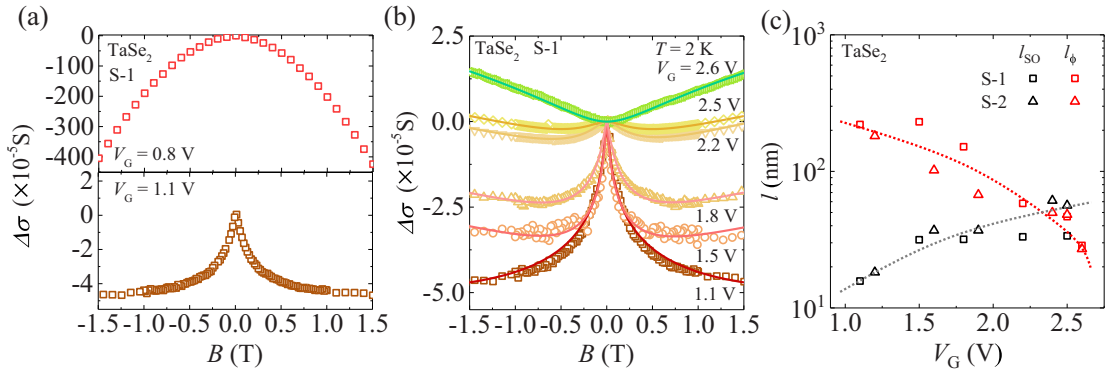

FIG. 3. Gate voltage tuned WAL-WL crossover. (a) Field dependent conductivity showed a parabolic curve at $T = 2$ K while it revealed WAL behavior after Li intercalation at $V_G = 1.1$ V. (b) MC of a 10-nm-thick sample at $V_G = 1.1$, 1.5, 1.8, 2.2, 2.5, and 2.6 V. All measurements were carried out at $T = 2$ K. The solid lines are fit to the MF theory. (c) Extracted electron-phonon scattering length l_φ and spin-orbital scattering length l_{so} as a function of V_G obtained from fitting the MF theory to data shown in (b). And l_{so} was found to increase from around 20 to 60 nm and l_φ decrease from around 400 to 30 nm as V_G was ramped from 0 to 2.5 V. The dashed line is guide to data points.

un-intercalated crystal of 2H-$TaSe_2$ was found previously to show WAL without SdHOs and $N = 6$ as well [37].

These observations suggest that the number of independent conduction channels was lowered from 6 to 2 as V_G increases. Incidentally, in the CDW state, the FS in 2H-$TaSe_2$ was found by ARPES measurements to be extremely complex because the onset of CDW leads to band folding and the opening of an energy gap on irregular parts of the FS, making its topology not fully resolved to date. The $N = 6$ result obtained from the quantum transport then provides an important parameter on the FS topology.

The interband scatterings are important for determining the property of a 2D electronic material, as seen in graphene in which the expected WAL due to a Berry phase of π would turn to WL because of the intriguingly consequential interband scatterings [38–40]. The $N = 6$ result for 2H-$TaSe_2$ suggests that interband scatterings are not present between any pair of FS pockets that are sufficiently well separated in the momentum space. This is unexpected at low gate voltage as sparsely intercalated 2H-$TaSe_2$ with a scattering potential varying at an atomic length scale should be able to facilitate large momentum transfer needed for interband scatterings. In any case, as V_G increases, the FS pockets around the K and the K' points (see the SM [31]) must have moved below the Fermi energy for $V_G \geqslant 1.1$ V, with the only remaining FS pocket being that of the largest holelike pocket near the Γ point. This would lead to the experimentally observed $N = 2$ result.

The Li ions intercalation induced variations in $l_\varphi^{-2} \sim \tau_j^{-1}$ and $l_{so}^{-2} \sim \tau_{so}^{-1}$ are clearly due to the change in FS topology. The spin-orbit scattering rate τ_{so}^{-1} is given by $2n_i u_{so}^2 \pi N(0)\overline{(k \times k')^2}$, where n_i is the density of impurities and u_{so} is the spin-orbit interaction potential, $N(0)$ is the density of states, k and k' are the crystal momenta for the two scattered charge carriers, and the bar represents the average over the FS [32]. Li intercalation will introduce disorder into the system, increasing n_i and both l_φ^{-1} and l_{so}^{-1} as a consequence. The Li ion intercalation into 2D crystals of 2H-$TaSe_2$ will also lower the Fermi energy, reducing the size of the FS, or Fermi wave vector, and ultimately the average $\overline{(k \times k')^2}$, leading to an increased l_{so}.

The temperature was also found to lead to a WAL-WL crossover. As shown in Figs. 5(a) and 5(c), negative MC was observed at $V_G = 1.5$ and 1.8 V, with its magnitude

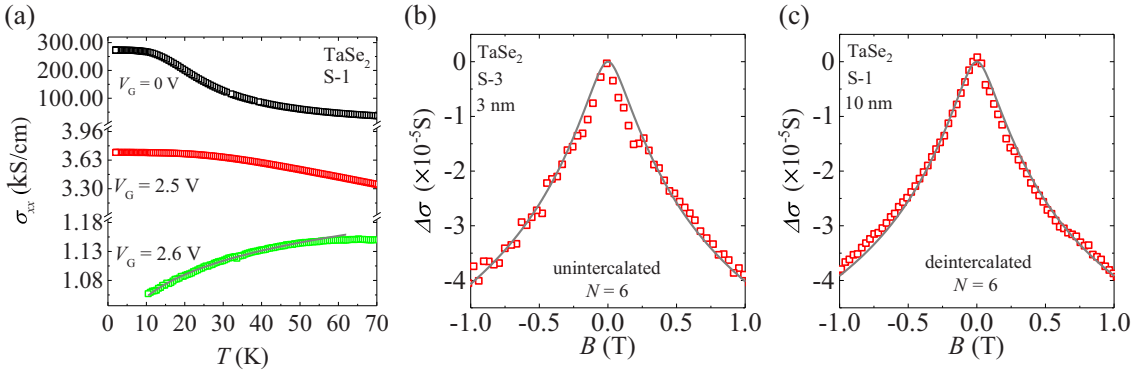

FIG. 4. Gate voltage tuned independent conduction channel. (a) Temperature dependence of sample conductance obtained at various gate voltages V_G as indicated, showing crossover between metallic and weakly localized behavior. Line in (a) is fit to logarithmic dependence. (b) MC of an un-intercalated 3-nm-thick sample and (c) a de-intercalated 10-nm-thick sample after the gate voltage V_G was swept from a high value back to 0 V.

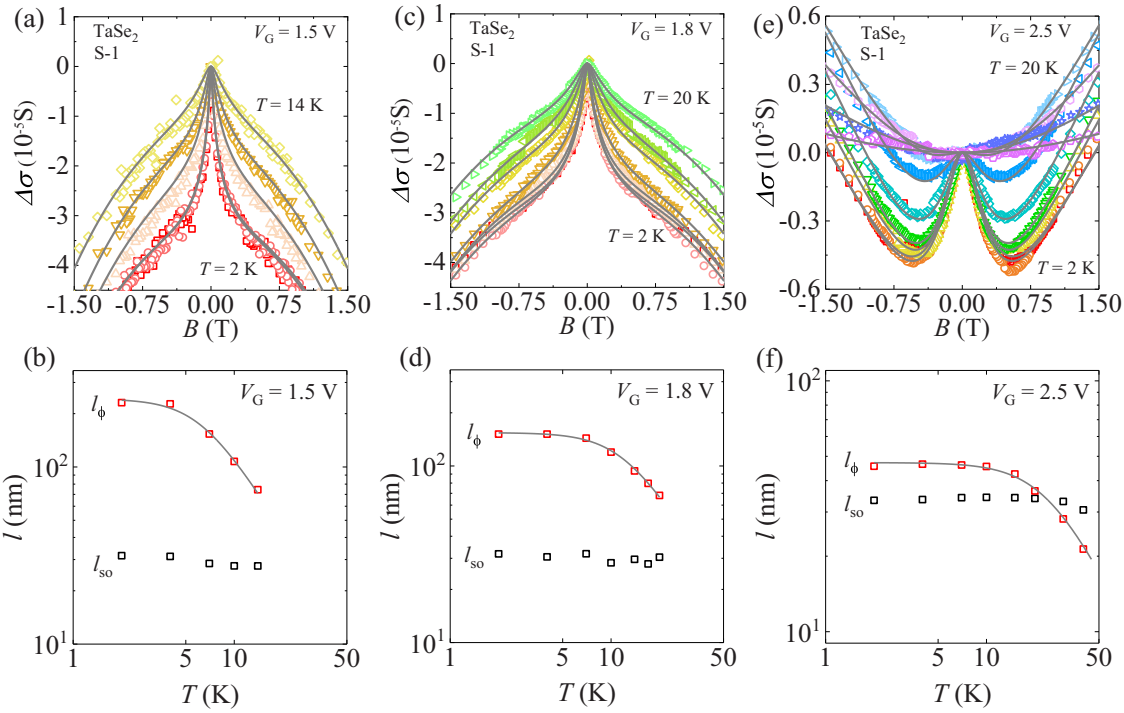

FIG. 5. Temperature tuned WAL-WL crossover. Magnetoconductance of the 10-nm-thick sample taken at (a) $V_G = 1.5$ V and $T = 2$, 4, 7, 10, and 14 K, (b) $V_G = 1.8$ V and $T = 2$, 4, 7, 10, 14, 17, and 20 K, and (c) $V_G = 2.5$ V and $T = 2$, 4, 7, 10, 15, 20, 30, 40, and 70 K. (d)–(f) Temperature dependence of fitting parameter B_φ and B_{so} obtained from fitting the MF theory to the data. Fitting values of B_φ to $A + BT^p$ was also shown. WL was found to persist to such a high temperature because even at $T = 70$ K and $V_G = 2.5$ V, at which we found $l_\varphi = 13$ nm.

decreasing with increasing temperature. At $V_G = 2.5$ V, a crossover between WL to WAL was seen as the temperature went up [Fig. 5(e)]. Given that $l_\varphi^2 = D\tau_\varphi$, $B_\varphi = \hbar/(4eD\tau_\varphi)$ we may fit the data shown in Figs. 5(b), 5(d), and 5(f) using $\tau_\varphi^{-1} = A + BT^p$. The best fit yielded a value of p in the range of 2.5–2.9. For electron-phonon scattering, the value of p is expected to be 2–4, suggesting that the main factor controlling l_φ is electron-phonon scattering. Similar results were obtained previously in graphene [39,40].

The decrease in electron-phonon scattering dominated l_φ as V_G was raised [Fig. 3(c)] suggest that the electron-phonon interaction is strengthened in 2D crystals of 2H-$TaSe_2$ by ion intercalation. Phonon spectrum calculations (see the SM [31]) suggest that Li intercalation hardens acoustic phonons. The soft acoustic phonon modes associated with the formation of the CDW disappeared in fully intercalated $LiTaSe_2$. The hardening of the phonons would tend to enhance the electron-phonon interaction. In addition, as suggested by the first-principles calculation, chemical bonds form between Li and Se ions—the hybridization between d and p orbitals (Fig. S4 in the SM [31]). The integration of Li ions into a 2D crystal of 2H-$TaSe_2$ appears to lead to an enhanced electron-phonon interaction because of the small mass of Li.

On the other hand, increasing V_G moves the Fermi energy towards the top of the band near Γ point, decreasing the size of the FS. This is consistent with the observation that R_H remains essentially a constant as a function of the magnetic field [Fig. 6(a)] and a constant of the temperature [Fig. 6(b)] while the corresponding carrier density dropping by two orders of magnitude as V_G increases [Fig. 6(c)]. The decreasing of the Fermi surface or the density of charge carriers tend to increase the effective Coulomb repulsion.

We found previously that T_c^{SC} was increased by over an order of magnitude from 0.15 K in the bulk to nearly 2 K in the Li ion intercalated 2D crystals [Fig. 2(c)] [41], which is direct evidence that the electron-phonon interaction is strengthened by the Li ion intercalation, through the combined effect of carrier doping and interlayer coupling. The present study suggests that this increase is due to the increase in the electron-phonon interaction matrix element as the electron-phonon scattering corresponds to its first-order and SC pairing the second-order effect (see the SM [31]). Interestingly, whether the enhancement of SC by ion intercalation observed previously in Cu intercalated $TiSe_2$ [16] and Li intercalated 1T-TaS_2 [42] is due to the enhancement of the electron-phonon interaction has not been resolved. Indeed, Sn or Cu intercalated 2H-$NbSe_2$ was found to show a suppressed rather than enhanced T_c^{SC} [43,44]. The present study is the first explicitly demonstrated example of ion-intercalation induced enhancement of SC originating from the strengthening of the electron-phonon interaction.

As noted above, the multi- to single-band change in FS topology deep in the CDW phase suggests that the formation of the CDW is unlikely related to the FS nesting. The dramatic change in the Raman spectrum deep in the CDW phase in 2H-$TaSe_2$, on the other hand, has important implication on the role played by the electron-phonon interaction in the formation of the CDW order, an issue considered previously

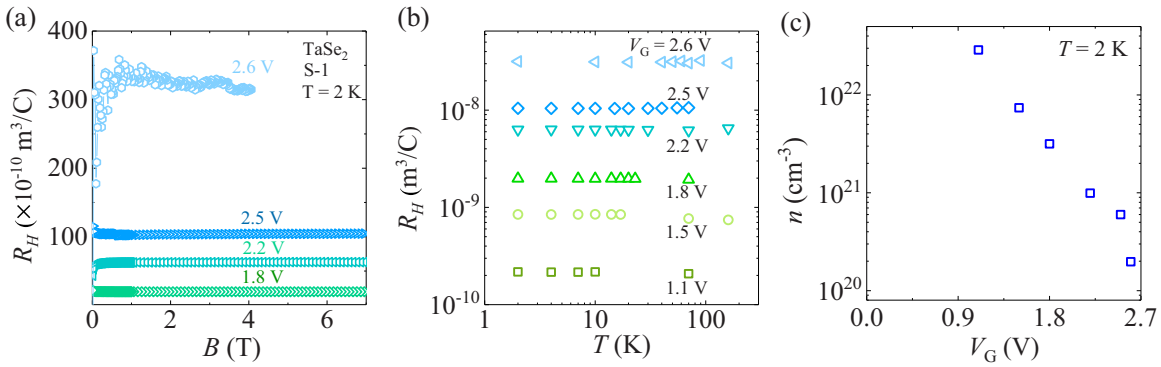

FIG. 6. Hall measurement and carrier density. (a) Hall coefficient R_H as a function of magnetic field at $V_G = 1.8$, 2.2, 2.5, and 2.6 V. (b) Temperature dependence of Hall coefficient at various V_G as indicated. (c) Hole densities estimated using a single-band model are 2.9×10^{22}, 7.4×10^{21}, 3.2×10^{21}, 9.1×10^{20}, 6.0×10^{20}, and 6.0×10^{20} cm^{-3} for $V_G = 1.1$, 1.5, 1.8, 2.2, 2.5, and 2.6 V, respectively.

[45]. The new insight provided by the present work is that the electron-phonon interaction is unlikely to be primarily responsible for the formation of CDW order in 2H-$TaSe_2$ either, given that the strengthening of the electron-phonon interaction by Li ion intercalation was already taking place when CDW order was hardly affected. The present work therefore raises an intriguing question on the mechanism for CDW in 2H-$TaSe_2$.

III. METHODS

A. Sample preparation

Single crystals of 2H-$TaSe_2$ were grown by the chemical vapor transport (CVT) method. A stoichiometric ratio of Ta and Se powder was mixed and put into a quartz tube, adding a small amount of iodine (∼20 mg) as transport agent. After being sealed under vacuum, the quartz tube was placed horizontally in a double zone furnace. The charge and the "cold" end were heated at 400 and 450 °C for 1 day, followed by elevated temperature to 850 and 750 °C for two weeks, respectively. The furnace was then shut down to allow it to cool down to room temperature before the quartz tube was opened to retrieve the crystals. Hexagonal platelike single crystals of $TaSe_2$ were found to be grown at the cold end of the quartz tube.

Atomically thin crystals of 2H-$TaSe_2$ were obtained by mechanical exfoliation and layer transfer using a silicone elastomer polydimethylsiloxane (PDMS) stamp and 300-nm-thick SiO_2/Si substrate [46]. The crystal thickness was estimated by a color code with the thickness of the crystal inferred from the color and faintness of the crystal. The color code was calibrated by atomic force microscope measurements. The device pattern was defined by standard photolithography, with the contacts prepared by the deposition of a 10-nm-thick Ti and 100-nm-thick gold film in series, followed by a lift-off process. Magnetoelectrical transport measurements were carried out down to 2 K on Hall bar shaped FET devices of multilayer 2H-$TaSe_2$ prepared using mechanical exfoliation and photolithography [Fig. 2(a)]. The electrodes were also covered by a photoresist layer to minimize the background. An electrolyte gate of $LiClO_4$/PEO was then applied, covering the $TaSe_2$ conduction channel and gate electrode, with the crystal sides exposed to the electrolyte.

B. Electrical transport measurements

The transport measurements were performed in a Quantum Design Physical Properties Measurement System. The system was able to reach a base temperature of 2 K and equipped with a magnet coil capable of sustaining fields up to 14 T. The source current and gate voltage were applied and probed with Keithley 2400 and 2182a. To take the measurements at certain Li concentration, the gate voltage is slowly ramped to a desired value at 330 K. We also waited for at least 1 h to allow Li ions to diffuse throughout the crystal to minimize the inhomogeneities before the sample was cooled down from 330 to 2 K at a constant rate, 1 K/min. A magnetic field was applied along the c axis of the crystal during the magnetotransport measurements.

ACKNOWLEDGMENTS

We acknowledge useful discussion with Antonio Garcia-Garcia, Jainedra Jain, Jingfeng Jia, Chaoxing Liu, and Zhe Wang. We thank Art Hebard and Tony Leggett for careful reading of the manuscript. The work done in China is supported by MOST of China (Grants No. 2015CB921104, No. 2014CB921201, and No. 2016YFA0301001), National Natural Science Foundation of China (Grants No. 11474198, No. 11521404, No. 91421304, and No. 11334006), the CAS/SAFEA international partnership program for creative research teams of China. Work at Penn State is supported by NSF under Grant No. EFMA1433378 and at Tulane supported by the U.S. Department of Energy under EPSCoR Grant No. DESC0012432 with additional support from the Louisiana Board of Regents. Hui Xing acknowledges additional support from a Shanghai talent program.

Y.L. and H.X. designed the experiment. J.L. and Z.M. grew the bulk 2H-$TaSe_2$. J.H. and H.L. carried out single crystal x-ray diffraction measurement. Y.W. fabricated the devices and performed electric measurements. C.L. and W.D. performed the first-principles calculation. Y.W., H.X., and Y.L. analyzed the data. All authors participated in the discussion of data. Y.L. and Y.W. wrote the paper.

[1] F. R. Gamble, J. H. Osiecki, M. Cais, R. Pisharody, F. J. DiSalvo, and T. H. Geballe, Intercalation complexes of Lewis bases and layered sulfides: A large class of new superconductors, Science **174**, 493 (1971).

[2] K. F. Mak, K. L. McGill, J. Park, and P. L. McEuen, The valley Hall effect in MoS_2 transistors, Science **344**, 1489 (2014).

[3] X. Xi *et al.*, Ising pairing in superconducting $NbSe_2$ atomic layers, Nat. Phys. **12**, 139 (2015).

[4] Y. Saito *et al.*, Superconductivity protected by spin–valley locking in ion-gated MoS_2, Nat. Phys. **12**, 144 (2016).

[5] X. Qian, J. Liu, L. Fu, and J. Li, Quantum spin Hall effect in two-dimensional transition metal dichalcogenides, Science **346**, 1344 (2014).

[6] Z. Fei *et al.*, Edge conduction in monolayer WTe, Nat. Phys. **13**, 677 (2017).

[7] S. Tang *et al.*, Quantum spin Hall state in monolayer $1T'-WTe_2$, Nat. Phys. **13**, 683 (2017).

[8] S Wu *et al.*, Observation of the quantum spin Hall effect up to 100 kelvin in a monolayer crystal, Science **359**, 76 (2018).

[9] X.-M. Zeng, H.-J. Yan, and C.-Y. Ouyang, First principles investigation of dynamic performance in the process of lithium intercalation into black phosphorus, Acta Phys. Sin. **61**, 247101 (2012).

[10] C. Julien, M. Jouanne, P. A. Burret, and M. Balkanski, Effects of lithium intercalation on the optical properties of InSe, Mater. Sci. Eng. B **3**, 39 (1989).

[11] A. Gugliuzza, A. Politano, and E. Drioli, The advent of graphene and other two-dimensional materials in membrane science and technology, Curr. Opin. Chem. Eng. **16**, 78 (2017).

[12] A. Ambrosi, Z. Sofer, and M. Pumera, Lithium intercalation compound dramatically influences the electrochemical properties of exfoliated MoS_2, Small **11**, 605 (2015).

[13] J. Shi, Y. Zhou, and S. Ramanathan, Colossal resistance switching and band gap modulation in a perovskite nickelate by electron doping, Nat. Commun. **5**, 4860 (2014).

[14] Y. Sun *et al.*, Strongly correlated perovskite lithium ion shuttles, Proc. Natl. Acad. Sci. USA **115**, 9672 (2018).

[15] A. M. Rappe, Ionic gating drives correlated insulator–metal transition, Proc. Natl. Acad. Sci. USA **115**, 9655 (2018).

[16] E. Morosan, H. W. Zandbergen, B. S. Dennis, J. W. G. Bos, Y. Onose, T. Klimczuk, A. P. Ramirez, N. P. Ong, and R. J. Cava, Superconductivity in Cu_xTiSe_2, Nat. Phys. **2**, 544 (2006).

[17] M. H. Van Maaren and G. M Schaeffer, Some new superconducting group V dichalcogenides, Phys. Lett. A **24**, 645 (1967).

[18] J. A. Wilson, F. J. Di Salvo, and S. Mahajan, Charge-Density Waves in Metallic, Layered, Transition-Metal Dichalcogenides, Phys. Rev. Lett. **32**, 882 (1974).

[19] D. E. Moncton, J. D. Axe, and F. J. DiSalvo, Study of Superlattice Formation in 2H-$NbSe_2$ and 2H-$TaSe_2$ by Neutron Scattering, Phys. Rev. Lett. **34**, 734 (1975).

[20] A. H. Castro Neto, Charge Density Wave, Superconductivity, and Anomalous Metallic Behavior in 2D Transition Metal Dichalcogenides, Phys. Rev. Lett. **86**, 4382 (2001).

[21] H. E. Brauer, H. I. Starnberg, L. J. Holleboom, H. P. Hughes, and V. N. Strocov, Na and Cs intercalation of 2H-$TaSe_2$ studied by photoemission, J. Phys.-Condens. Matter **13**, 9879 (2001).

[22] A. König, K. Koepernik, R. Schuster, R. Kraus, M. Knupfer, B. Büchner, and H. Berger, Plasmon evolution and charge-density wave suppression in potassium intercalated 2H-$TaSe_2$, Europhys. Lett. **100**, 27002 (2012).

[23] M. Eibschutz, D. Salomon, D. W. Murphy, S. Zahurak, and J. V. Waszczak, Direct observation of charge transfer in lithium-intercalated 2H-$TaSe_2$ by ^{181}Ta Mössbauer spectroscopy, Chem. Phys. Lett. **135**, 591 (1987).

[24] J. C. Tsang and M. W. Shafer, Raman spectroscopy of intercalated layered structure compounds, Solid State Commun. **25**, 999 (1978).

[25] Y. Wu *et al.*, Lithium ion intercalation in thin crystals of hexagonal $TaSe_2$ gated by a polymer electrolyte, Appl. Phys. Lett. **112**, 023502 (2018).

[26] R. M. Fleming and R. V. Coleman, Oscillatory magnetotransport in the layer compounds $4H_b$-TaS_2 and 2H-$TaSe_2$, Phys. Rev. B **16**, 302 (1977).

[27] S. V. Borisenko, A. A. Kordyuk, A. N. Yaresko, V. B. Zabolotnyy, D. S. Inosov, R. Schuster, B. Bchner, R. Weber, R. Follath, L. Patthey, and H. Berger, Pseudogap and Charge Density Waves in Two Dimensions, Phys. Rev. Lett. **100**, 196402 (2008).

[28] Y. W. Li, J. Jiang, H. F. Yang, D. Prabhakaran, Z. K. Liu, L. X. Yang, and Y. L. Chen, Folded superstructure and degeneracy-enhanced band gap in the weak-coupling charge density wave system 2H-$TaSe_2$, Phys. Rev. B **97**, 115118 (2018).

[29] J. A. Yan, M. A. Cruz, B. Cook, and K. Varga, Structural electronic and vibrational properties of few-layer 2H- and 1T-$TaSe_2$, Sci. Rep. **5**, 16646 (2015).

[30] M. Naito and S. Tanaka, Galvanomagnetic effects in the charge-density-wave state of 2H-$NbSe_2$ and 2H-$TaSe_2$, J. Phys. Soc. Jpn. **51**, 228 (1982).

[31] See Supplemental Material at http://link.aps.org/supplemental/10.1103/PhysRevMaterials.3.104003 for more information about the transport, Raman and first principles calculation results of Li intercalated $TaSe_2$.

[32] S. Maekawa and H. Fukuyama, Magnetoresistance in two-dimensional disordered systems: Effects of Zeeman splitting and spin-orbit scattering, J. Phys. Soc. Jpn. **50**, 2516 (1981).

[33] D. Rainer and G. Bergmann, Multiband effects in weak localization, Phys. Rev. B **32**, 3522 (1985).

[34] H. Yuan *et al.*, Zeeman-type spin splitting controlled by an electric field, Nat. Phys. **9**, 563 (2013).

[35] P. A. Lee and T. V. Ramakrishnan, Disordered electronic systems, Rev. Mod. Phys. **57**, 287 (1985).

[36] G. Bergmann, Weak localization in thin films: A time-of-flight experiment with conduction electrons, Phys. Rep. **107**, 1 (1984).

[37] A. T. Neal, Y. Du, H. Liu, and P. D Ye, Two-dimensional TaSe metallic crystals: Spin–orbit scattering length and breakdown current density, ACS Nano **8**, 9137 (2014).

[38] H. Suzuura and T. Ando, Crossover from Symplectic to Orthogonal Class in a Two-Dimensional Honeycomb Lattice, Phys. Rev. Lett. **89**, 266603 (2002).

[39] F. V. Tikhonenko, A. A. Kozikov, A. K. Savchenko, and R. V. Gorbachev, Transition between Electron Localization and Antilocalization in Graphene, Phys. Rev. Lett. **103**, 226801 (2009).

[40] S. Das Sarma, S. Adam, E. H. Hwang, and E. Rossi, Electronic transport in two-dimensional graphene, Rev. Mod. Phys. **83**, 407 (2011).

[41] Y. Wu, J. He, J. Liu, H. Xing, Z-Q. Mao, and Y. Liu, Dimensional reduction and ionic gating induced enhancement

of superconductivity in atomically thin crystals of 2H-$TaSe_2$, Nanotechnology **30**, 035702 (2019).

[42] Y. Yu *et al.*, Gate-tunable phase transitions in thin flakes of 1T-TaS_2, Nat. Nanotechnol. **10**, 270 (2015).

[43] S. Naik, G. K. Pradhan, S. G. Bhat, B. C. Behera, P. S. Anil Kumar, S. L. Samal, and D. Samal, The effect of Sn intercalation on the superconducting properties of 2H-$NbSe_2$, Phys. C **561**, 18 (2019).

[44] H. Luo, J. Strychalska-Nowak, J. Li, J. Tao, T. Klimczuk, and R. J. Cava, S-shaped suppression of the superconducting transition temperature in Cu-intercalated $NbSe_2$, Chem. Mater. **29**, 3704 (2017).

[45] P. Monceau, Electronic crystals: An experimental overview, Adv. Phys. **61**, 325 (2012).

[46] C.-G. Andres *et al.*, Deterministic transfer of two-dimensional materials by all-dry viscoelastic stamping, 2D Materials **1**, 011002 (2014).